JOURNAL OF THERMOPHYSICS AND HEAT TRANSFER
Vol. 20, No. 4, October–December 2006

Heat/Mass Transfer with Circular Pin Fins in Impingement/Effusion Cooling System with Crossflow

Sung Kook Hong,* Dong-Ho Rhee,* and Hyung Hee Cho†
Yonsei University, Seoul 120-749, Republic of Korea

DOI: 10.2514/1.16864

The purpose of the present study is to investigate the local heat/mass transfer characteristics with circular pin fins in the impingement/effusion cooling with an initial crossflow. The results are compared with those for the cases without pin fins and with rib turbulators. The pin fins are installed between two perforated plates and the crossflow passes between these two plates. A blowing ratio is changed from 0.5 to 1.5 for the fixed jet Reynolds number of 10,000. The local heat/mass transfer coefficients on the effusion plate are measured using a naphthalene sublimation method. When circular pin fins are installed in the impingement/effusion system, heat/mass transfer is augmented due to the generation of vortex and wake. Especially, locally low heat/mass transfer regions in front of the effusion hole are reduced. Because pin fins divert the crossflow passing in the injection hole region, the wall jet is less swept away than the case without pin fins, which results in the increase of heat/mass transfer. As the blowing ratio increases, the pin fins lead to higher heat/mass transfer than the case without pin fins. Compared with rib turbulators, the pin fins yield lower average Sh value at $M = 1.0$ but higher average Sh value at other blowing ratios.

Nomenclature

D_h	=	hydraulic diameter of test channel
D_{cp}	=	diameter of circular pin fin
D_{naph}	=	mass diffusion coefficient of naphthalene vapor in air
d	=	injection and effusion hole diameter
H	=	gap distance between injection and effusion plates
h_m	=	local mass transfer coefficient
I	=	local momentum flux ratio of crossflow and impinging jets, $\rho_c V_c^2/\rho_i V_i^2$
M	=	blowing ratio (total mass flow ratio of crossflow and impinging jets), Q_c/Q_i, Eq. (1)
MR	=	local mass flux ratio of crossflow and impinging jets, $\rho_c V_c/\rho_i V_i$
$\dot{m}$	=	local naphthalene mass transfer per unit area and time, Eq. (2)
$\underline{Nu}$	=	Nusselt number based on the hole diameter, hd/k
$\overline{Nu}_{cp}$	=	Average Nusselt number based on the circular pin fin diameter, hD_{cp}/k
P_{hole}	=	pitch of array holes
Pr	=	Prandtl number
Q_c	=	flow rate of crossflow
Q_i	=	flow rate of injected jet or effused flow
Re_{cp}	=	Reynolds number based on circular pin fin diameter and maximum flow velocity in the channel
Re_d	=	Reynolds number based on hole diameter and average velocity in the hole
Re_{Dh}	=	Reynolds number based on hydraulic diameter of channel and average velocity of crossflow
Sc	=	Schmidt number
Sh	=	Sherwood number based on the hole diameter, Eq. (3)
$\overline{\overline{Sh}}$	=	overall averaged Sherwood number
S_L	=	longitudinal distance for pin fin arrangements
S_T	=	transverse distance for pin fin arrangements
t	=	thickness of injection and effusion plates
V_c	=	mean velocity of crossflow
V_i	=	mean velocity of impinging jet
x, z	=	distance from the center of an effusion hole
$\Delta P_{\text{channel}}$	=	differential pressure between the inlet and the exit of the channel
ΔP_{jet}	=	differential static pressure between the injection and effusion plenum chambers
Δt	=	test duration, Eq. (2)
Δy	=	naphthalene sublimation depth per unit area during the experiment, Eq. (2)
ρ_c	=	density of crossflow
ρ_i	=	density of impinging jet flow
ρ_s	=	density of solid naphthalene, Eq. (2)
$\rho_{v,w}$	=	naphthalene vapor density at the surface, Eq. (2)
$\rho_{v,\infty}$	=	naphthalene vapor density of the incoming flow, Eq. (2)

Received 28 March 2005; revision received 28 September 2005; accepted for publication 29 October 2005.

*Department of Mechanical Engineering.
†Department of Mechanical Engineering; hhcho@yonsei.ac.kr.

Introduction

IN order to achieve high thermal efficiency, modern gas turbine engines are designed to operate at very high temperature, which requires proper cooling techniques to protect the components of the gas turbines. Therefore, various cooling methods such as film cooling, jet impingement cooling, and convective internal passage cooling have been developed. Among the cooling schemes, an impingement/effusion cooling is one of the advanced cooling techniques for combustor liner or turbine parts cooling. This technique combines two cooling schemes, that is, array jet impingement and film cooling. Therefore, the inner surfaces of hot components are cooled by the impingement of cooling air, and outer surfaces that are in contact with hot gases are protected by effusion film cooling (Fig. 1). For this advantage, the investigations on the impingement/effusion cooling technique have been performed for the last few decades.

Hollwarth and Dagan [1] and Hollwarth et al. [2] examined average and local heat transfer coefficients on the effusion surface, and reported that arrays with staggered vents consistently yield higher heat transfer rates than do the impinging jets on the solid plates. Nazari and Andrews [3] studied the film cooling performance with the effects of the number of holes for impingement/effusion

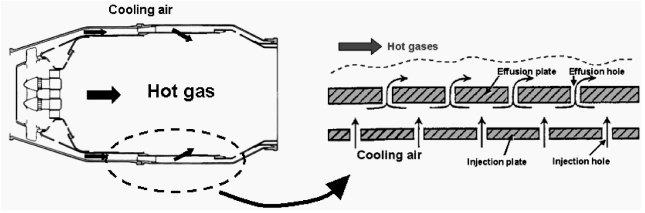

Fig. 1 Schematic view of impingement/effusion cooling in a combustor liner.

cooling. Cho and Goldstein [4] investigated the effect of hole arrangements on local heat/mass transfer characteristics inside the effusion plate. They reported that the overall transfer rate is approximately 45–55% higher than that for the impingement cooling alone. Cho and Rhee [5] and Rhee et al. [6] also investigated heat/mass transfer and flow characteristics of an impingement/effusion cooling system with various experimental conditions, such as gap distance, Reynolds number, and hole arrangement and size.

In actual situations such as combustor liner and turbine parts cooling, an initial crossflow is generated in the internal passages and the crossflow significantly affects the heat transfer characteristics in the passages. Hence, several studies have concentrated on the crossflow effect. Metzger and Korstad [7], Bebahani and Goldstein [8], Florschuetz et al. [9], Haiping et al. [10], Rhee et al. [11], Bailey and Bunker [12], Gao et al. [13], and Huang et al. [14] investigated the effects of crossflow on array jet impingements with various conditions, and reported that the crossflow has an adverse effect. However, these studies have been focused on array jet impingement cooling.

For the impingement/effusion cooling system with crossflow, Ekkad et al. [15] investigated the effect of crossflow orientation and showed that the crossflow orientation with small crossflow leads to high heat transfer distributions. Rhee et al. [16] performed the experiment and examined the effects of the crossflow on heat transfer. They reported that the overall heat/mass transfer rates on the effusion (target) plate decrease as the crossflow rate increases, which is a similar trend to array jet impingement. Also, they found that locally low transfer regions are formed between the adjacent effusion holes.

In general, because it is difficult to control the amount of crossflow in the cooling system, it is important to reduce the adverse effect of the crossflow at the fixed operating conditions. For this purpose, the studies using ribs on the target or effusion plate have been conducted. Haiping et al. [17,18] performed the experiments with various test conditions for jet impingement cooling on a rib-roughened surface. Andrews et al. [19] investigated the effects of the direction of the transverse rib with respect to the crossflow for impingement cooling, and reported that the rib turbulators change the effects of crossflow and the enhancement of heat transfer is achieved with ribs. Rhee et al. [20] applied various rib configurations to the impingement/effusion cooling system and reported that averaged heat transfer increased 4–15% compared with the case without ribs.

For the same purpose, circular pin fins are considered to be one of the possible methods to reduce the adverse effect of the crossflow and to improve the cooling performance and durability. Also, using pin fins has additional advantages such as heat conduction through the pin fins and enhancement of structural strength of the system. However, there have been only a few studies on pin fins in the impingement/effusion cooling. Andrews et al. [21] and Annerfeldt et al. [22] performed the experiments with pin fins but those were confined to the jet impingement cooling. Funazaki et al. [23] and Yamawki et al. [24] investigated the effects of circular pin fins on the impingement/effusion cooling but did not consider the crossflow.

Therefore, in the present study, the effects of circular pin fins on heat/mass transfer characteristics on the effusion plate are investigated for the impingement/effusion cooling with an initial crossflow. These results are compared with the case without pin fins and the case with rib turbulators. Also, the effects of the blowing ratio (crossflow rate) are investigated.

A naphthalene sublimation method is used to measure the detailed local heat/mass transfer coefficients on the effusion plate. One of the great advantages of this technique is accurate and easy imposition of isothermal or adiabatic boundary conditions in convective heat transfer without conductive and radiative losses.

Experimental Apparatus and Conditions

Experimental Apparatus

Figure 2a shows the experimental apparatus, which is composed of three parts: impinging jet, flow effusion, and crossflow supply parts. The impinging jet and crossflow are supplied into the test section by a blowing-type blower (blower 1) and the effusion flow is discharged by a suction-type blower (blower 2). Three orifice flow meters are installed to measure the flow rates of the crossflow, the injected jets, and the effused flow, respectively.

The schematics of the test section and the effusion plate are presented in Figs. 2b and 2c. The crossflow channel is located between the injection and the effusion plenum chambers, and jets from injection holes impinge on the effusion plate and then discharge through the effusion holes to simulate the impingement/effusion cooling. Cho and Goldstein [25] reported that heat/mass transfer coefficients on the inside surface of the effusion plate are the same with and without mainstream over the outer surface of the effusion

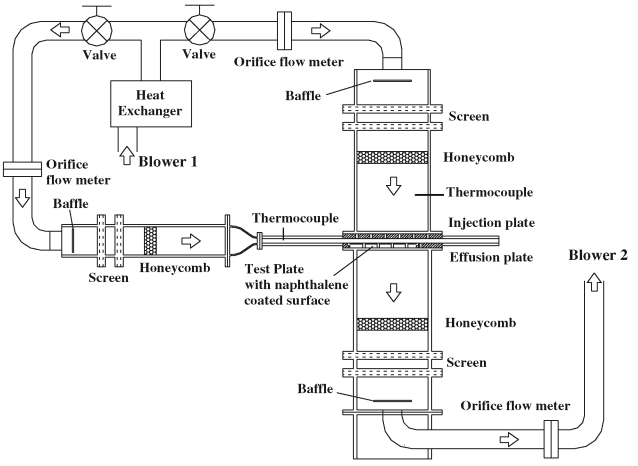

a) Experimental apparatus

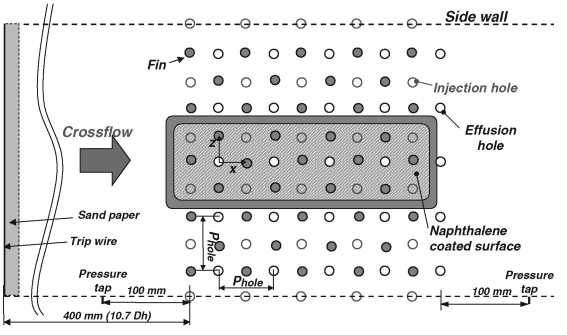

b) Test section, top view

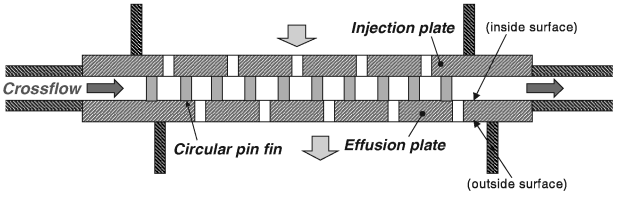

c) Test section, side view

Fig. 2 Schematic view of experimental facility.

plate. Therefore, the effect of mainstream is not considered in the present study.

The cross section of the channel is 300 mm (W) × 20 mm (H), and the hydraulic diameter of the channel is 37.5 mm. The distance between the inlet of the channel and the first row of injection holes is set to be 400 mm ($10.7D_h$). To obtain the turbulent channel flow, sand paper and trip wire are installed at the inlet of the channel after the contraction section with a 6:1 area ratio.

The diameter of the injection and the effusion holes is 10 mm, and the thickness of the plates is 20 mm ($t/d = 2.0$). Each plate has 25 (5×5) holes of square array, and the ratio of hole spacing to the diameter (P_{hole}/d) is 6.0. A staggered hole arrangement between the injection and the effusion plates is used in this study. The gap distance between the injection and the effusion plate is fixed at $H/d = 2.0$ for all the tested cases.

A naphthalene-coated test plate is installed on the effusion plate for local mass transfer measurements as shown in Fig. 2b. Four effusion holes are located in the test plate and these holes are protected with the aluminum rim to maintain the circular hole shape. The naphthalene-coated area in the test plate is $8.4 \times 28d$ and a T-type thermocouple is installed on the test plate to measure the naphthalene surface temperature, which is needed to obtain naphthalene vapor density on the surface.

To measure pressure drop through the crossflow channel, inlet and outlet pressure taps are installed at the sidewall 100 mm away from the first row of injection holes and the last row of effusion holes, respectively. Also, the static pressure at the injection and effusion plenum chambers is measured to get the pressure drop across the perforated plates. In this study, a differential pressure sensor (LPE 9145 model, Druck) was used to measure the differential static pressure.

Pin Fin Arrangements

Figure 3 shows the schematic diagram of circular pin fin arrangements. In the present study, five different pin fin arrangements are considered and those are referred to as CP0, CP1, CP2, CP1U, and CP1D, respectively. For all cases, circular pin fins are installed along the centerline of the effusion holes, as shown in Figs. 3a–3e. For the CP1 case, another row of circular pin fins is installed along the centerline of the injection holes. For the CP2 case, two additional rows of circular pin fins are positioned $1d$ away from the centerline of the injection holes. Therefore, the number of installed pin fins for CP1 and CP2 corresponds to two and three times that for CP0, respectively.

For CP1U and CP1D, the number of installed pin fins is the same as that for CP1 but the position of pin fins along the centerline of the injection holes is different. The characters U and D mean that the circular pin fins are installed at upstream and downstream positions of the injection hole as shown in Figs. 3d and 3e, respectively.

The diameter of the circular pin fin is 10 mm and the height of the pin fin is equal to the channel height. As shown in Fig. 3, the longitudinal and transverse spacing of pin fins ranges from 1.5 to $6D_{cp}$ and the parameters of each case are listed in Table 1.

In the present study, the results with rib turbulators by Rhee et al. [20] are presented to compare and evaluate various enhancement techniques that could apply to the impingement/effusion cooling system with crossflow. Figure 3f shows a schematic of rib turbulators installed on the effusion plate. The rectangles indicate the transverse rib turbulators of rectangular cross section (3×3 mm) and rib turbulators are installed with the rib spacing of $3d$.

Operating Conditions

In this study, to investigate the effects of the crossflow, the flow rate (velocity) of the crossflow through the channel is changed with a fixed flow rate of impinging jets. A blowing ratio has been used to represent the influence of crossflow on the cooling system. The blowing ratio is a ratio of total flow rate of crossflow to the impinging jets and defined as Eq. (1):

$$M = Q_c/Q_i \tag{1}$$

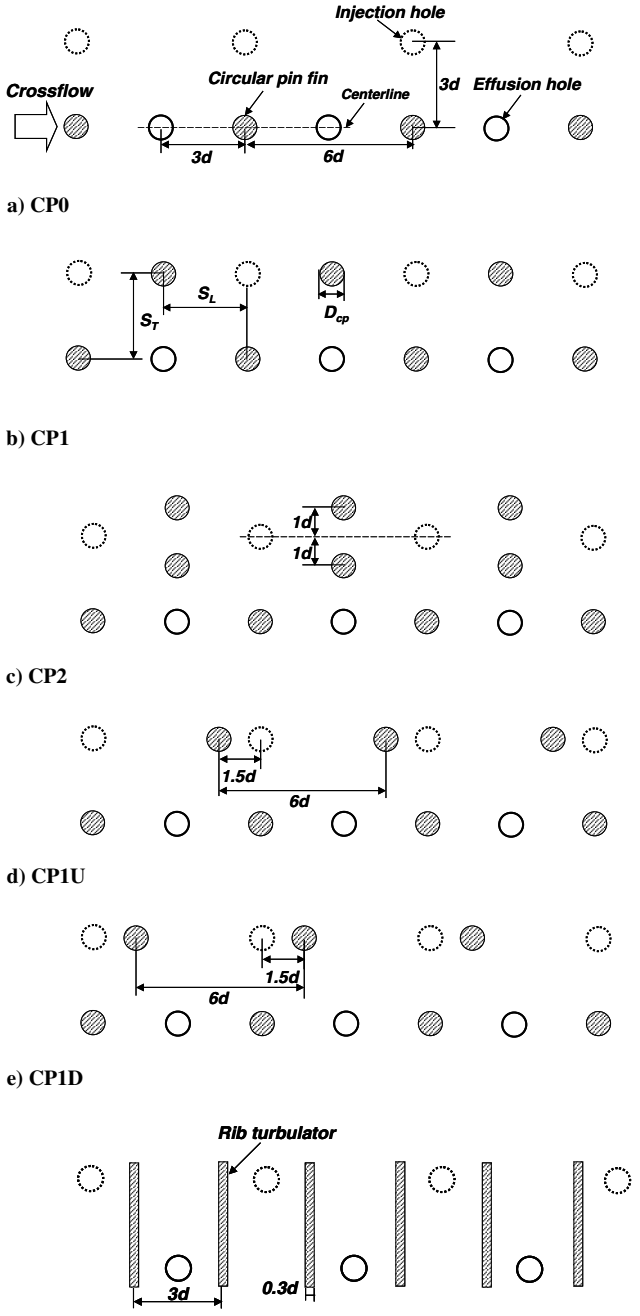

Fig. 3 Schematic view of various circular pin fin arrangements.

The experiments were performed for the blowing ratio from 0.5 to 1.5 ($Re_{Dh} = 6,000$–$18,000$), and the desired conditions were obtained by changing the flow rate of the crossflow with the fixed flow rate of impinging jets. For the impingement/effusion cooling, the flow rate of air through the effusion holes is set to be the same as that through the injection holes to catch the effects of crossflow precisely. A local mass flux ratio and momentum ratio based on the blowing ratio range from 0.164 to 0.491 and from 0.027 to 0.241, respectively. The operating conditions are listed in Table 2.

Data Reduction

The local mass transfer coefficient is defined as

$$h_m = \frac{\dot{m}}{\rho_{v,w} - \rho_{v,\infty}} = \frac{\rho_s(\Delta y/\Delta t)}{\rho_{v,w}} \tag{2}$$

because the incoming flow contains no naphthalene, $\rho_{v,\infty} = 0$ in the

Table 1 Pin fin arrangement parameters.

Case	CP0	CP1	CP2	CP1U	CP1D
S_L (mm)	60	30	30	15&45	15&45
S_T (mm)	60	30	20	30	30

Table 2 Operating conditions.

M	MR	I	Re_d	Re_{Dh}
0.5	0.164	0.027	10,000	6,130
1.0	0.327	0.107	10,000	12,270
1.5	0.491	0.241	10,000	18,400

present study, therefore the mass transfer coefficients are calculated from sublimation depth, naphthalene vapor density, and solid naphthalene density. The details of the measuring system are described by Rhee et al. [16]. The Sherwood number, a dimensionless form of mass transfer coefficient, is used to present the heat/mass transfer results and can be expressed as

$$Sh = h_m d / D_{\text{naph}} \tag{3}$$

Note that for the channel flow cases (the simple channel cooling), the hydraulic diameter of the channel was used as a characteristic length ($Sh_{Dh} = h_m D_h / D_{\text{naph}}$). The properties of naphthalene suggested by Goldstein and Cho [26] are used in the present study.

The mass transfer coefficients can be converted to the heat transfer coefficients using the heat and mass transfer analogy by Eckert [27]. The Prandtl number is 0.71 for air and the Schmidt number is 2.28 for the naphthalene vapor in air at 25°C. The experiments were conducted at room temperature, and the Lewis number (Pr/Sc) for this study is about 0.31.

$$Nu/Sh = (\text{Pr}/\text{Sc})^{0.4}, \qquad Nu = 0.624Sh \tag{4}$$

The comparison between heat transfer and mass transfer results is presented by Rhee et al. [16]. Uncertainty of the Sherwood numbers using the method of Kline and McClintock [28] for single sample experiments, considering the measured surface temperature, depth, position, and correlation equations, is within ±7.1% in the entire operating range of the measurement, based on a 95% confidence interval. This uncertainty is mainly attributed to the uncertainty of the properties of naphthalene, such as the naphthalene saturated vapor density (3.8%) and diffusion coefficient of naphthalene vapor in air (5.1%). In contrast, the error due to the depth measurement is only 0.7%. The other uncertainties are 1.1% and 4.9% for density of solid naphthalene and mass transfer coefficient, respectively.

To estimate the pressure drop in the impingement/effusion cooling system, a ratio of pressure drop through the channel to that across the perforated plates ($\Delta P_{\text{cross}}/\Delta P_{\text{jet}}$) was presented. From these results, one can assess the additional pressure loss with pin fins and predict its effects on the operation of the cooling system.

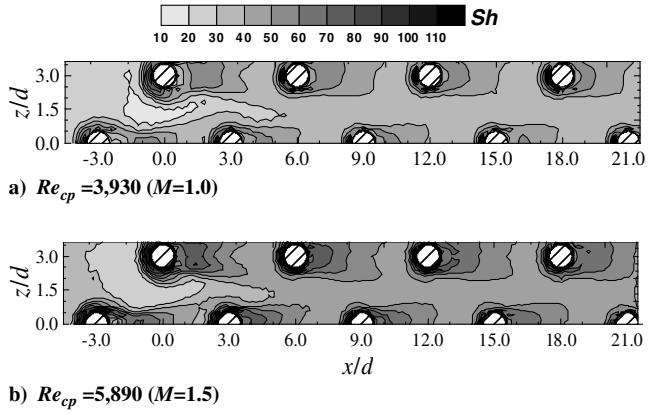

a) Re_{cp} =3,930 (M=1.0)

b) Re_{cp} =5,890 (M=1.5)

Fig. 4 Contour plots of *Sh* for crossflow only with circular pin fins at different Reynolds numbers.

Results and Discussion

In the present study, the local heat/mass transfer characteristics with circular pin fins in the impingement/effusion cooling with crossflow are investigated. The results are compared with the heat/mass transfer patterns for the simple channel cooling (crossflow only) and the impingement cooling of the jet array, which are also tested for baseline data.

Simple Channel Cooling with Pin Fins

For the baseline data and the qualification test, the simple channel flow with CP1 pin fin arrangement is tested at different channel Reynolds numbers, which correspond to $M = 1.0$ and 1.5 for the array jet impingement or the impingement/effusion cooling.

Figure 4 presents the contours of *Sh* for the simple channel cooling with pin fins. As reported in the previous investigations [29,30], the heat/mass transfer characteristics by the generation of horseshoe vortices and wake are observed. High heat/mass transfer appears in front of the pin fin on the endwall (effusion plate) due to the horseshoe vortex. Just downstream of the pin fin, the relatively low *Sh* distributions are observed because of a flow recirculation with low local velocity. But farther downstream, the heat/mass transfer is enhanced considerably due to the increase of flow disturbance. Therefore, the augmentation of heat/mass transfer generally appears in the wake region that is formed behind the pin fin. As shown in Fig. 4b, the heat/mass transfer patterns around the pin fins are

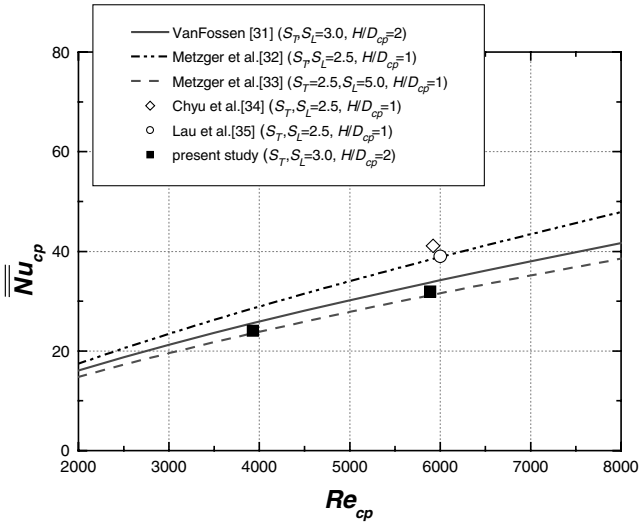

Fig. 5 Comparison of average Nusselt numbers of circular pin fins at different Reynolds numbers.

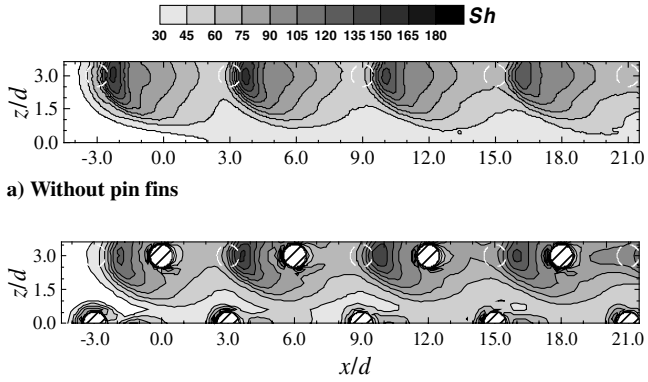

a) Without pin fins

b) With pin fins (CP1 case)

Fig. 6 Contour plots of *Sh* for array jet cooling with initial crossflow at $M = 1.0$.

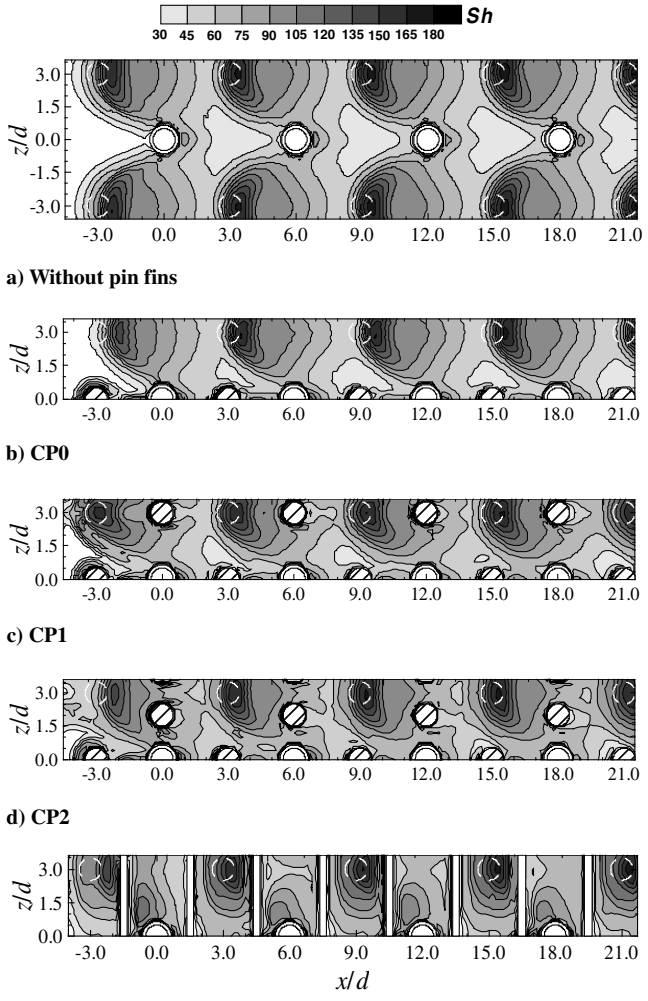

a) Without pin fins

b) CP0

c) CP1

d) CP2

e) 90DU rib turbulators (Rhee et al. [20])

Fig. 7 Contour plots of *Sh* for impingement/effusion cooling with circular pin fins at $M = 1.0$.

maintained with higher Reynolds numbers but the levels of *Sh* distributions are higher due to the increase of crossflow velocity.

Figure 5 shows averaged Nusselt numbers at various Reynolds numbers with other data suggested by VanFossen [31], Metzger et al. [32,33], Chyu et al. [34], and Lau et al. [35]. The Nusselt numbers of the present study are converted from the Sherwood numbers using the heat and mass transfer analogy. The Reynolds number is based on the maximum average velocity and the diameter of the circular pin fin. Note that the maximum average velocity represents the mean velocity in minimum flow area induced by the installation of pin fins. As shown in the plot, our data are slightly lower than other results except the result of Metzger et al. [33] ($S_T = 2.5$, $S_L = 5.0$). This is because our pin spacing is larger and then the effect of the pin decreases. However, our results are in good agreement with the correlation of VanFossen [31] for the same pin spacing.

Array Jet Cooling with Initial Crossflow

For array jet impingement, the contour plots of *Sh* at $M = 1.0$ are presented in Fig. 6. In the contour plots, the white dotted circles represent the projected positions of the injection holes and hatched circles indicate the circular pin fins installed in the channel. For an array jet impingement cooling without pin fins (Fig. 6a), because the spent air from impinging jets is added to the crossflow, the effects of the crossflow become stronger as the flow moves downstream. Therefore, the stagnation points of the impinging jets shift downstream and the peak values decrease with increasing x/d. Moreover, at the midway region ($z/d \cong 0.0$), heat/mass transfer is much lower than that in the stagnation region because the wall jet, which is the developing flow in an outward radial direction from the stagnation region, is swept by the crossflow and the boundary layer develops along the midway region.

When the pin fins are installed (Fig. 6b), the *Sh* distributions have the combined features induced by the array jet and pin fin. In the injection region ($z/d \cong 3.0$), except the first injection hole, the stagnation points of impinging jets shift less downstream and the levels of *Sh* distributions are higher than those for the case without pin fins. This is because the effects of the crossflow along $z/d \cong 3.0$ are weakened by the pin fins. At the midway region ($z/d \cong 0.0$), the effects of the crossflow are dominant and the high horseshoe-shaped distributions of *Sh* are formed clearly around the pin fins.

Impingement/Effusion Cooling with Crossflow

Effects of Circular Pin Fins

Figure 7 presents the contour plots of *Sh* for the impingement/effusion cooling with pin fins at $M = 1.0$ (including the case without pin fins). For the comparison of pin fins, the result with rib turbulators by Rhee et al. [20] is also presented. White dotted circles and small half circles (full circles for the case without pin fins) represent the projected positions of the injection holes and the effusion holes with the aluminum rim between two half circles, respectively. Also hatched circles and half circles indicate the circular pin fins installed in the channel.

For the case without pin fins, the *Sh* distributions are nonuniform and asymmetric because the injected jet is deflected and the wall jet is swept away by the crossflow. Therefore, wall jets do not cover the upstream regions of the stagnation points and heart-shaped low transfer regions are formed between the effusion holes. Meanwhile, the contour represents a periodic distribution, except the first row of injection holes, because a certain amount of the crossflow and spent air is discharged through the effusion holes and balance between flow inlet and outlet in the channel is conserved.

When the pin fins are installed in the channel, the change of *Sh* distributions is observed in the effusion region ($z/d \cong 0.0$). The pin fin generates the vortex and wake, promoting the flow mixing and increasing the local turbulence. Therefore, locally low heat/mass transfer regions are reduced at the upstream of the effusion holes.

The CP0 case (Fig. 7b) shows that the positions of stagnation points shift more downstream whereas *Sh* distributions are very similar to those for the case without pin fins in the injection region ($z/d \cong 3.0$). This is because the pin fin reduces the cross-sectional area at injection hole positions ($x/d = -3$, 3, 9, 15, and 21) and increases the effect of crossflow.

The contour plots of CP1 and CP2 are shown in Figs. 7c and 7d, respectively. For both cases, high *Sh* distributions spread more upstream (negative x direction) than those for the case without pin fins. Especially, for the CP2 case, locally high heat/mass transfer regions expanded more laterally (both z directions). This mainly results from the blockage effect that the pin fin obstructs the crossflow and prevents the wall jet from being swept away. In the effusion region ($z/d \cong 0.0$) and midway region ($z/d \cong 1.0$) for

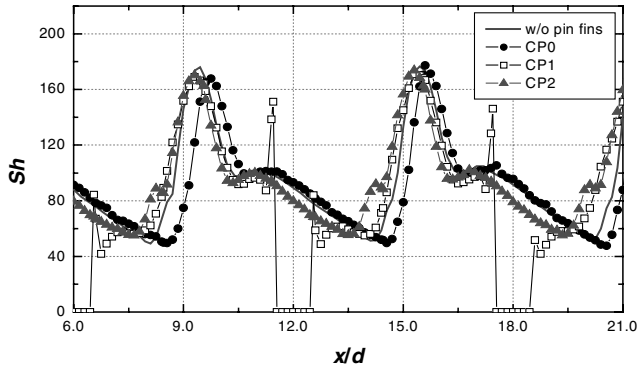

a) z/d =3.0

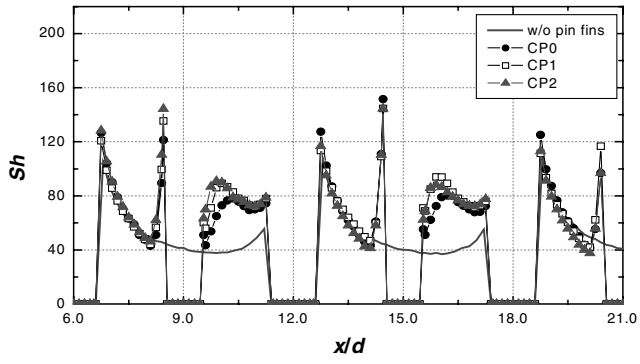

b) z/d =0.0

Fig. 8 Local distributions of *Sh* for impingement/effusion cooling with circular pin fins at $M = 1.0$.

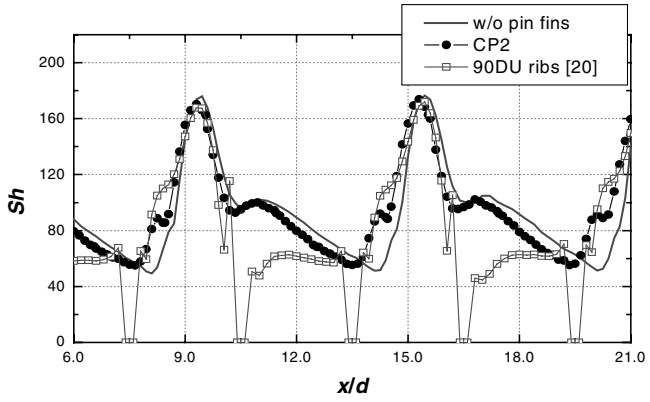

Fig. 9 Comparison of pin fins with rib turbulators at local distributions of *Sh* along $z/d = 3.0$.

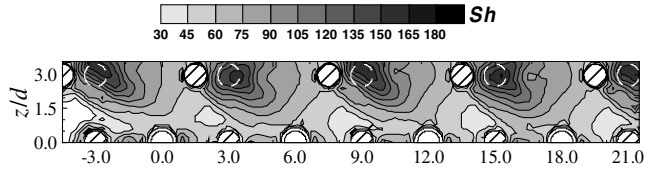

a) CP1U

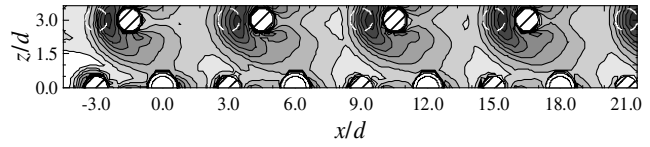

b) CP1D

Fig. 10 Contour plots of *Sh* for impingement/effusion cooling at different pin fin arrangements.

CP2, higher *Sh* are observed than for other cases with pin fins. This is attributed to the increase of flow mixing induced by short pin spacing S_T. Moreover, additional heat transfer enhancement is expected due to larger surface enlargement and heat conduction induced by the increase of installed pin fins.

To compare with the circular pin fins, the contour of the case with rib turbulators is presented in Fig. 7e. White, long rectangles represent the transverse rib turbulators installed on the effusion surface. Owing to the effects of rib turbulators such as blocking the near-wall crossflow and flow reattachment behind the rib turbulator, the heat/mass transfer pattern is different from that for the cases with pin fins. These transverse rib turbulators make the wall jet spread more widely in the lateral direction although the wall jet does not develop downstream and the recirculating flow is formed behind the rib turbulator. Compared with the circular pin fins, higher *Sh* values are observed widely at the interrib regions of the injection hole (e.g., $7.5 < x/d < 10.5$) whereas relatively low *Sh* values appear at the interrib regions of the effusion hole (e.g., $10.5 < x/d < 13.5$). The flow suction through the effusion hole accelerates local flow around the effusion holes. Moreover, this flow suction promotes the reattachment of the flow passing over the ribs. Therefore, locally high heat/mass transfer regions (e.g., $z/d \cong 1.0$ and $x/d \cong 11.5$) are formed.

As shown in the contour plots, the pin fin relates to the wall jet partially in the region of the installed pin fin whereas the rib turbulators have interaction with the wall jet in the entire region, which induces the difference of overall *Sh* distributions.

Figure 8 represents the local *Sh* distributions for the case with and without pin fins. As shown in the contour plots, the *Sh* distributions have periodic pattern in the overall region except the inlet region including the first injection hole. Therefore, to observe the effects of the pin fin on local heat/mass transfer more clearly, the data in the range of $6.0 < x/d < 21.0$ are presented. In the local plots, the value of zero indicates the position of installed pin fins or effusion holes.

The local values along the centerline of the injection holes ($z/d = 3.0$) are presented in Fig. 8a. For all cases, the levels of peak values at stagnation points are almost the same and Sh values decrease as the boundary layer develops after impingement. Moreover, at the downstream region of the stagnation point, the secondary peaks appear about $2d$ away from the stagnation point due to the flow transition of the wall jet to turbulent flow. However, at the upstream region of the stagnation point, the secondary peaks are hardly observed because of the interaction with the crossflow.

For the CP0 case, the stagnation points shift about $0.3d$ downstream, compared with other cases. This is caused by the increased crossflow effect. When pin fins are installed along $z/d = 3.0$ (CP1 case), the strong vortex produces additional peaks in front of the pin fins ($x/d \cong 11.5$ and 17.5) whereas the recirculating flow leads to low *Sh* values just behind the pin fins. The CP2 case has higher values at the upstream region of the stagnation point. However, the *Sh* values are lower than those for the case without pin fins at the downstream region because the wall jet spreads more toward the lateral direction and the effect of the wall jet along $z/d = 3.0$ decreases.

Along $z/d = 0.0$ (Fig. 8b), all CP cases show similar *Sh* distributions because the pin fins are installed at the same positions ($x/d = 9$, 15 and 21). Behind the pin fins, CP cases have 40–55% higher values than the case without pin fins due to the increased flow disturbance. Around the effusion holes ($x/d \cong 6$, 12, and 18), the locally high values of *Sh* are obtained because the flow at those regions is accelerated and disturbed.

Figure 9 shows the local *Sh* distributions along $z/d = 3.0$ for the case with rib turbulators and CP2. In the plot, the value of zero indicates the position of installed rib turbulators. As expected in the contour plots, the local *Sh* distributions for the case with rib turbulators are different from those for CP2. At the interrib regions of the injection hole (e.g., $7.5 < x/d < 10.5$), high *Sh* values are observed in the upstream region of stagnation point because the rib turbulator in front of the injection hole prevents the near-wall crossflow and then the wall jet spreads well toward the upstream direction. However, at the interrib regions of effusion hole (e.g.,

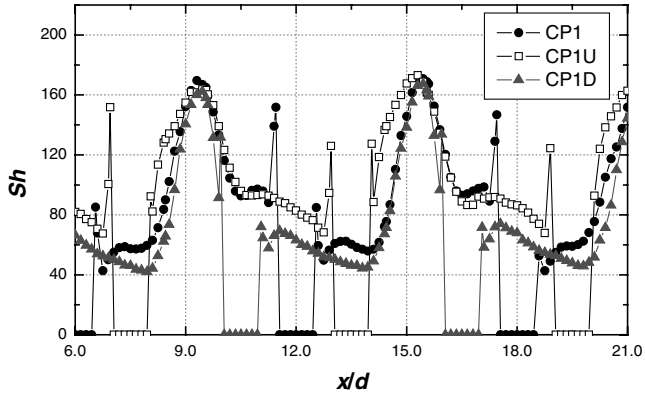

Fig. 11 Local distributions of *Sh* along the centerline of injection holes at different pin fin arrangements.

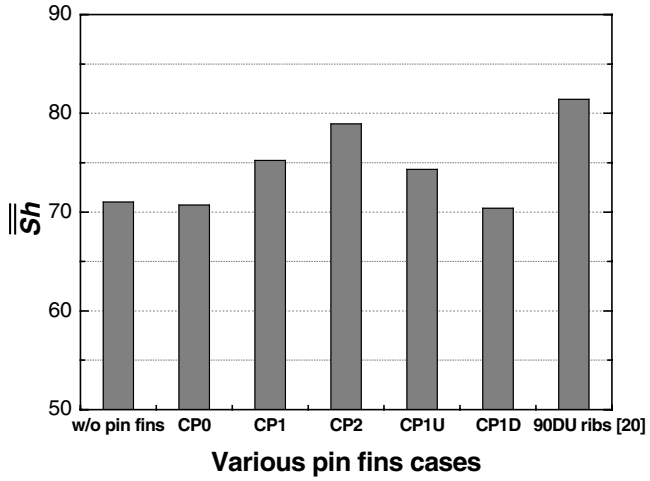

Fig. 12 Overall averaged *Sh* for various cases with pin fins at $M = 1.0$.

$10.5 < x/d < 13.5$), the rib turbulator behind the injection hole prevents the wall jet from spreading downstream and produces the recirculation flow, so that *Sh* values are lower than those for CP2.

Effects of Pin Fin Position

In the present study, two different pin fin positions on the basis of CP1 configuration are investigated to protect the impinging jets from the crossflow and to reduce the low heat/mass transfer regions more effectively. As shown in Fig. 10, the local heat/mass transfer characteristics vary with the change of pin fin position along the centerline of the injection holes ($z/d = 3.0$).

For CP1U, because the pin fins installed along $z/d = 3.0$ block the crossflow just in front of the impinging jets, the stagnation regions are formed more upstream than those for other cases. The wake induced by the pin fin disappears because the wall jet spreads behind the pin fin. Therefore, the CP1U case produces a little enhancement of heat/mass transfer in the injection region. However, the accelerated crossflow around the pin fin strongly pushes the wall jet downstream and then the wall jet does not develop well in the lateral direction. Hence, in the midway region ($z/d \cong 1.5$), *Sh* distributions are similar to those for CP1. It is shown that parts of the stagnation regions are slightly away from the centerline of the injection hole. This is possibly attributed to the discrepancy of the centerline between the pin and the impinging jet: when the center of the pin is positioned in the upward region of the centerline of the injection holes (i.e., $z/d > 3.0$), on the basis of crossflow approaching the impinging jet, a smaller amount of crossflow passes in the upward region ($z/d > 3.0$) than in the downward region ($z/d < 3.0$). Also the center of low-pressure distributions just behind the pin is formed in the upward region ($z/d > 3.0$). So the impinging jet is deflected in the upward region ($z/d > 3.0$) and then an asymmetric *Sh* pattern appears.

When the pin fins are installed just behind the impinging jets (CP1D case), the injected flow directly meets the pin fin and the wall jet spreads around the pin fin. Compared with other cases, the wall jet spreads more toward the lateral direction from the stagnation region. However, this wall jet developing laterally collides with the crossflow and is swept away downstream, which does not enhance the heat/mass transfer in the midway and effusion regions. Moreover, the stagnation zone is reduced and locally low heat/mass transfer occurs behind the pin fin. The reason is that the pin fin blocks the wall jet passing along $z/d = 3.0$ and most of the wall jet spreads into the surrounding area as mentioned.

Figure 11 presents the local *Sh* distributions along $z/d = 3.0$. For CP1U, the higher *Sh* values are obtained at the upstream region of the stagnation point than for CP1 due to strong blockage effect. In contrast, the CP1D case has low *Sh* values, especially at the downstream region of the stagnation point. This is because the wall jet developing along $z/d = 3.0$ is blocked by the pin fin, although the flow mixing due to wake increases, which means that *Sh* reduction caused by blocking of the wall jet is greater than *Sh* augmentation by wake. Therefore, it is found that a pin fin position like CP1D is not good for enhancing the heat/mass transfer in the injection region.

The area-averaged *Sh* values for various cases at $M = 1.0$ are shown in Fig. 12. The averaged values are calculated by averaging local data in the range of $-3.0 \leq x/d \leq 21.0$ and $0 \leq z/d \leq 3.0$. It is noted that the averaged values at the inlet region ($-3.0 \leq x/d \leq 3.0$) are about 10% lower than those from other regions.

As expected in the local *Sh* distributions, the CP1, CP1U, and CP2 configurations have 5–11% higher values than the case without pin fins. Among the tested cases with circular pin fins, CP2 has the highest averaged *Sh* value. The reason is that the increase of the number of installed pin fins strengthens the blockage effect and flow disturbance. In contrast, CP0 and CP1D have similar values to the case without pin fins although the heat/mass transfer are enhanced in the effusion region. This is attributed to the fact that the pin fin strengthens the effect of the crossflow for CP0 and blocks the spreading of the wall jet for CP1D, decreasing the heat/mass transfer in the injection region.

As shown in Fig. 12, the case with rib turbulators yields a higher averaged value than pin fin cases, because long transverse ribs protect the wall jet from being swept away by the crossflow in the entire region, and heat/mass transfer enhancement due to flow reattachment is added. On the contrary, the circular pin fins protect the wall jet from the crossflow only behind the region of the installed pin fins, inducing weaker blockage effect in the whole region compared with rib turbulators. However, the pin fins have merits such as larger surface enlargement and heat conduction. So, the additional heat transfer augmentation is expected with pin fins.

Effects of Blowing Ratio

In this study, the experiments were carried out with various blowing ratios from 0.5 to 1.5 for CP1 and CP2 to investigate the effects of the blowing ratio (crossflow rate). For the case without pin fins, which are reported in [16], the level of *Sh* at the stagnation region becomes lower as the blowing ratio increases. Also low heat/mass transfer region between effusion holes enlarges.

Figures 13 shows the contours of the CP1 case at $M = 0.5$ and $M = 1.5$, respectively. At a low blowing ratio of $M = 0.5$, the stagnation regions are not affected significantly by the crossflow and the wall jet spreads well on the whole effusion plate except in the vicinity of the effusion hole. The heat/mass transfer on the effusion plate is slightly affected by the pin fins because of a low-channel Reynolds number. However, at a high blowing ratio of $M = 1.5$, the influence of pin fins becomes greater, leading to the heat/mass transfer enhancement around the pin fin as shown in simple channel flow case (Fig. 4). The stagnation point and the wall jet greatly shift downstream by the strong crossflow. Behind the effusion hole, the

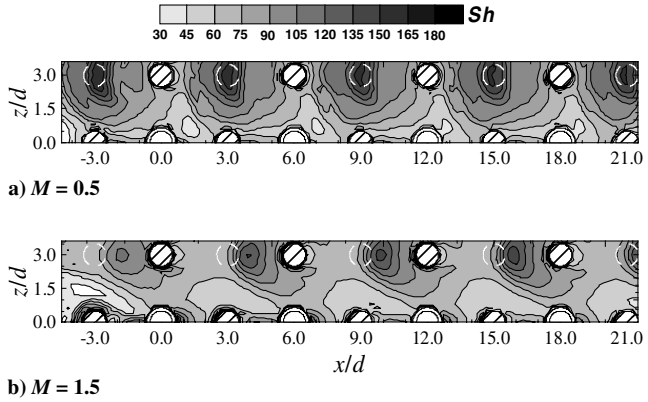

a) $M = 0.5$

b) $M = 1.5$

Fig. 13 Contour plots of *Sh* for impingement/effusion cooling with pin fins at different blowing ratios (CP1 case).

high *Sh* values are observed due to the strong reattachment of the channel crossflow with suction into the effusion hole [36].

Local *Sh* distributions along $z/d = 3.0$ are presented in Fig. 14. At the low blowing ratio of $M = 0.5$, the stagnation points are found at the center of the injection hole ($x/d = 9$, 15 and 21) and the secondary peaks due to flow transition to turbulence are also observed clearly. However, as the blowing ratio increases, these secondary peaks disappear and the positions of stagnation points move downstream. For the case of $M = 1.0$, the level of stagnation point is the highest because the turbulence intensity increases by interaction between the injected jet and the crossflow. At the high blowing ratio of $M = 1.5$, the level of stagnation point decreases and the position of that shifts more downstream. However, in the wake region, the strong crossflow ($M = 1.5$) induces slightly higher *Sh* values than those for the case of $M = 1.0$.

Figure 15 presents the overall average *Sh* values at various blowing ratios. In the case without pin fins, as the blowing ratio increases, the averaged value decreases considerably due to the adverse effect of the crossflow. The cases with pin fins show the similar feature. However, higher averaged values are obtained than for the case without pin fins due to the influence of pin fins. Especially, at $M = 1.5$, the cases with pin fins have 16–22% enhancement for averaged *Sh* values.

Compared with rib turbulators, lower averaged values are obtained at the blowing ratio of $M = 1.0$. This is attributed to the partial blockage effect by pin fins as mentioned before. However, the cases with pin fins have higher values than the case with rib turbulators at a low blowing ratio of $M = 0.5$. The reason is that rib turbulators act as obstacles to the wall jet, confining the wall jet in the region between the installed rib turbulators as reported in [20] whereas the pin fins do not confine the wall jet. With increasing the blowing ratio from 1.0 to 1.5, the reduction of averaged *Sh* for the cases with pin fins is smaller than that for rib turbulators. This is because the impinging jet is less swept away downstream, in other words, the pin fin installed in front of the injection hole protects the impinging jet from the crossflow better than the rib turbulator in the channel. Therefore, it is found that the CP2 configuration is effective in a wide range of $M = 0.5$ to 1.5 and rib turbulators give the highest enhancement at the specific condition ($M = 1.0$) for averaged *Sh* value.

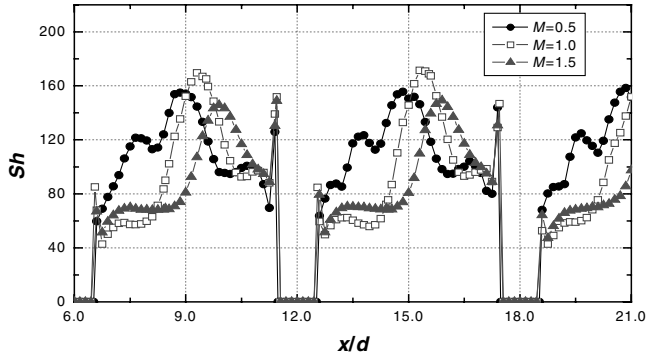

Fig. 14 Local distributions of *Sh* along $z/d = 3.0$ at different blowing ratios.

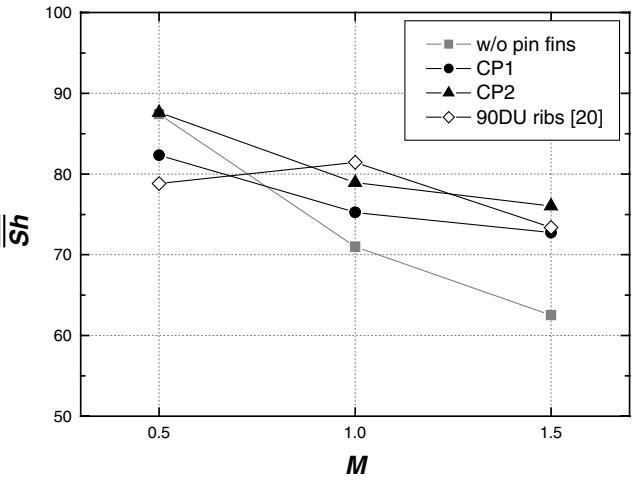

Fig. 15 Overall averaged *Sh* for various cases with pin fins at different blowing ratios.

Pressure Loss

In the present study, the pressure drop in the crossflow channel was measured to investigate pressure loss in the channel having the pin fins. The pressure drop through the channel is normalized by the pressure difference between the injection and effusion plenum chambers, that is, a ratio of pressure drop through the channel to that across the perforated plates ($\Delta P_{\text{cross}}/\Delta P_{\text{jet}}$). From these pressure measurements, one can assess the additional pressure loss with pin fins and predict its effects on the operation of the cooling system. Figure 16 presents the results at various blowing ratios. The value for the case with rib turbulators is also presented to compare with pin fins.

It is shown that the pressure drop becomes greater as the blowing ratio increases, that is, the Reynolds number of the channel flow increases. For the case without pin fins, the pressure drop through the channel is less than 10% of that across the perforated plates. On the contrary, for the cases with pin fins, the pressure drop through the channel increases considerably due to the reduction of the cross-sectional area. Pressure loss becomes higher with increasing the number of installed pin fins. In particular, the pressure loss of CP2 is approximately three–four times higher than that without pin fins.

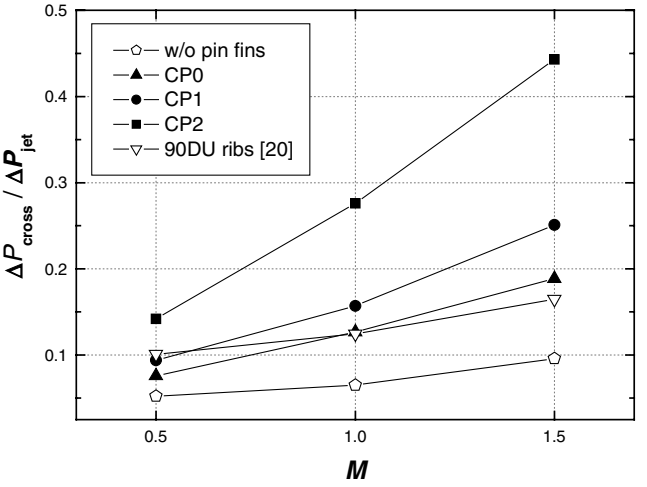

Fig. 16 Pressure drop ratios for the impingement/effusion cooling at various cases with pin fins.

Compared with rib turbulators, the cases with pin fins induce greater pressure loss, which means that the circular pin fins need more pumping power to obtain the same flow rate in the impingement/effusion cooling system.

Although it is accompanied by high pressure loss, the pin fins have additional favorable effects: surface enlargement, heat conduction through the pin fins, and enhancement of structural strength in the system. The installation of pin fins could give more effective cooling performance than that of ribs in an impingement/effusion cooling system where more pressure loss is acceptable or structural strength of system is required. Meanwhile, the rib turbulators are preferable to the pin fins when low pressure is needed.

Conclusion

The present study investigates the local heat/mass transfer characteristics with circular pin fins in the impingement/effusion cooling with crossflow. The results are compared with those for the cases without pin fins and with rib turbulators. The results of this study can be summarized as follows:

1) When circular pin fins are installed in the channel, locally low heat/mass transfer regions are reduced due to the generation of vortex and wake. Moreover, the pin fins prevent the wall jet from being swept away, increasing the local heat/mass transfer in the injection region.

2) The alteration of pin fin positions along the centerline of the injection hole affects the impinging jet and wall jet directly, resulting in the change of local heat/mass transfer distributions. When the pin fins are installed in front of the impinging jet, the blockage effect on the crossflow enhances the heat/mass transfer. However, the pin fins installed just behind the impinging jet block the wall jet, decreasing the heat/mass transfer.

3) Using the circular pin fins, the overall heat/mass transfer increases 5–11% than that for the case without pin fins at $M = 1.0$. The increase of installed pin fins leads to the augmentation of the overall Sh value. However, despite the installation of pin fins, the CP0 and CP1D cases have little enhancement of overall Sh value.

4) At the low blowing ratio of $M = 0.5$, the overall Sh values are similar to the case without pin fins. As the blowing ratio increases, higher Sh values are obtained compared with the case without pin fins, producing 16–22% enhancement of overall Sh value at $M = 1.5$.

5) Compared with rib turbulators, the cases with pin fins have lower average Sh values due to the partial blockage effect at $M = 1.0$. However, CP2 configuration yields higher average Sh values at other blowing ratios because the pin fins block the wall jet less at $M = 0.5$ and protect the impinging jet from the crossflow more effectively at $M = 1.5$ than the rib turbulators.

6) Pressure drop through the channel becomes greater as the number of installed pin fins and the blowing ratio increases. Although the pressure loss through the channel is less than 10% of that across the perforated plates for the case without pin fins, the pressure loss of the CP2 case is approximately three–four times higher than that without pin fins. Compared with rib turbulators, the pressure loss by the pin fins becomes higher as the blowing ratio increases.

Acknowledgment

The authors wish to acknowledge support for this study by the Korean Ministry of Science and Technology through the National Research Laboratory program.

References

[1] Hollwarth, B. R., and Dagan, L., "Arrays of Impinging Jets with Spent Fluid Removal Through Vent Holes on the Target Surface Part 1: Average Heat Transfer," *Journal of Engineering for Power*, Vol. 102, No. 4, 1980, pp. 994–999.

[2] Hollwarth, B. R., Lehmann, G., and Rosiczkowski, J., "Arrays of Impinging Jets with Spent Fluid Removal Through Vent Holes on the Target Surface Part 2: Local Heat Transfer," *Journal of Engineering for Power*, Vol. 105, No. 2, 1983, pp. 393–402.

[3] Nazari, A., and Andrews, G. E., "Impingement/Effusion Cooling: Influence of Number of the Holes and Pressure Loss on Film and Heat Transfer Coefficient," *Proceedings of the 7th International Gas Turbine Congress*, Vol. 2, 1999, pp. 638–648.

[4] Cho, H. H., and Goldstein, R. J., "Effect of Hole Arrangements on Impingement/Effusion Cooling," *Proceedings of the 3rd Korean Society of Mechanical Engineers–Japan Society of Mechanical Engineers Thermal Engineering Conference*, 1996, pp. 71–76.

[5] Cho, H. H., and Rhee, D. H., "Local Heat/Mass Transfer Measurement on the Effusion Plate in Impingement/Effusion Cooling System," *Journal of Turbomachinery*, Vol. 123, No. 3, 2001, pp. 601–608.

[6] Rhee, D. H., Choi, J. H., and Cho, H. H., "Heat (Mass) Transfer on Effusion Plate in Impingement/Effusion Cooling Systems," *Journal of Thermophysics and Heat Transfer*, Vol. 17, No. 1, 2003, pp. 95–102.

[7] Metzger, D. E., and Korstad, R. J., "Effects of Cross Flow in Impingement Heat Transfer," *Journal of Engineering for Power*, Vol. 94, No. 1, 1972, pp. 35–41.

[8] Behbahani, A. I., and Goldstein, R. J., "Local Heat Transfer to Staggered Arrays of Impinging Circular Air Jets," *Journal of Engineering for Power*, Vol. 105, No. 2, 1983, pp. 354–360.

[9] Florschuetz, L. W., Metzger, D. E., and Su, C. C., "Heat Transfer Characteristics for Jet Array Impingement with Initial Crossflow," *Journal of Heat Transfer*, Vol. 106, No. 1, 1984, pp. 34–41.

[10] Haiping, C., Wanbing, C., and Taiping, H., "3-D Numerical Simulation of Impinging Jet Cooling with Initial Crossflow," American Society of Mechanical Engineers, Paper 99-GT-256, 1999.

[11] Rhee, D. H., Yoon, P. H., and Cho, H. H., "Local Heat/Mass Transfer and Flow Characteristics of Array Impinging Jets with Effusion Holes Ejecting Spent Air," *International Journal of Heat and Mass Transfer*, Vol. 46, No. 6, 2003, pp. 1049–1061.

[12] Bailey, J. C., and Bunker, R. S., "Local Heat Transfer and Flow Distributions for Impinging Jet Arrays of Dense and Sparse Extent," American Society of Mechanical Engineers, Paper GT-2002-30473, 2002.

[13] Gao, L., Ekkad, S. V., and Bunker, R. S., "Impingement Heat Transfer Under Linearly Stretched Arrays of Holes," American Society of Mechanical Engineers, Paper GT-2003-38178, 2003.

[14] Huang, Y., Ekkad, S. V., and Han, J. C., "Detailed Heat Transfer Distributions Under an Array of Orthogonal Impinging Jets," *Journal of Thermophysics and Heat Transfer*, Vol. 12, No. 1, 1998, pp. 73–79.

[15] Ekkad, S. V., Huang, Y., and Han, J. C., "Impingement Heat Transfer on a Target Plate with Film Cooling Holes," *Journal of Thermophysics and Heat Transfer*, Vol. 13, No. 4, 1999, pp. 522–528.

[16] Rhee, D. H., Choi, J. H., and Cho, H. H., "Flow and Heat (Mass) Transfer Characteristics in an Impingement/Effusion Cooling System with Crossflow," *Journal of Turbomachinery*, Vol. 125, No. 1, 2003, pp. 74–82.

[17] Haiping, C., Dalin, Z., and Taiping, H., "Impingement Heat Transfer from Rib Roughened Surface Within Arrays of Circular Jets: the Effects of the Relative Position of the Jet Hole to the Ribs," American Society of Mechanical Engineers, Paper 97-GT-331, 1997.

[18] Haiping, C., Jingyu, Z., and Taiping, H., "Experimental Investigation on Impingement Heat Transfer from Rib Roughened Surface Within Arrays of Circular Jets: Effect of Geometric Parameters," American Society of Mechanical Engineers, Paper No. 98-GT-208, 1998.

[19] Andrews, G. E., Abdul Hussain, R. A. A., and Mkpadi, M. C., "Enhanced Impingement Heat Transfer: Comparison of Co-flow and Cross-flow with Rib Turbulators," *Proceedings of IGTC2003*, Paper No. IGTC2003Tokyo TS-075, 2003.

[20] Rhee, D. H., Nam, Y. W., and Cho, H. H., "Local Heat/Mass Transfer with Various Rib Arrangements in Impingement/Effusion Cooling System with Crossflow," *Journal of Turbomachinery*, Vol. 126, No. 4, 2004, pp. 615–626.

[21] Andrews, G. E., Abdul Hussain, R. A. A., and Mkpadi, M. C., "Enhanced Impingement Heat Transfer: The Influence of Impingement X/D for Interrupted Rib Obstacles (Rectangular Pin Fins)," American Society of Mechanical Engineers, Paper GT-2004-54184, 2004.

[22] Annerfeldt, M. O., Persson, J. L., and Torison, T., "Experimental Investigation of Impingement Cooling with Turbulators or Surface Enlarging Elements," American Society of Mechanical Engineers, Paper 2001-GT-0149, 2001.

[23] Funazaki, K., Tarukawa, Y., Kudo, T., Mastsuno, S., Imai, R., and Yamawki, S., "Heat Transfer Characteristics of an Integrated Cooling Configuration for Ultra-High Temperature Turbine Blades: Experimental and Numerical Investigations," American Society of Mechanical Engineers, Paper 2001-GT-0148, 2001.

[24] Yamawki, S., Nakamata, C., Imai, R., Mastsuno, S., Yoshida, T., Mimura, F., and Kumada, M., "Cooling Performance of an Integrated Impingement and Pin Fin Cooling Configuration," American Society of

Mechanical Engineers, Paper GT-2003-38215, 2003.
[25] Cho, H. H., and Goldstein, R. J., "Heat (Mass) Transfer and Film Cooling Effectiveness with Injection Through Discrete Holes—Part 1: Within Holes and on the Back Surface," *Journal of Turbomachinery*, Vol. 117, No. 3, 1995, pp. 440–450.
[26] Goldstein, R. J., and Cho, H. H., "A Review of Mass Transfer Measurement Using Naphthalene Sublimation," *Experimental Thermal and Fluid Science*, Vol. 10, No. 4, 1995, pp. 416–434.
[27] Eckert, E. R. G., *Analogies to Heat Transfer Processes, in Measurements in Heat Transfer*, edited by E. R. G. Eckert and R. J. Goldstein, Hemisphere, New York, 1976, pp. 397–423.
[28] Kline, S. J., and McClintock, F., "Describing Uncertainty in Single Sample Experiments," *Mechanical Engineering*, Vol. 75, No. 1, 1953, pp. 3–8.
[29] Goldstein, R. J., Chyu, M. K., and Hain, R. C., "Measurement of Local Mass Transfer on a Surface in the Region of the Base of a Protruding Cylinder with a Computer-Controlled Data Acquisition System," *International Journal of Heat and Mass Transfer*, Vol. 28, No. 5, 1985, pp. 977–985.
[30] Won, S. Y., Mahmood, G. I., and Ligrani, P. M., "Spatially-Resolved Heat Transfer and Flow Structure in a Rectangular Channel with Pin Fins," *International Journal of Heat and Mass Transfer*, Vol. 47, No. 8, 2004, pp. 1731–1743.
[31] VanFossen, G. J., "Heat Transfer Coefficients for Staggered Arrays of Short Pin Fins," *Journal of Engineering for Power*, Vol. 104, No. 2, 1982, pp. 268–274.
[32] Metzger, D. E., Berry, R. A., and Bronson, J. P., "Developing Heat Transfer in Rectangular Ducts with Staggered Arrays of Short Pin Fins," *Journal of Heat Transfer*, Vol. 104, No. 4, 1982, pp. 700–706.
[33] Metzger, D. E., Shepard, W. B., and Haley, S. W., "Row Resolved Heat Transfer Variations in Pin Fin Arrays Including Effects of Non-Uniform Arrays and Flow Convergence," American Society of Mechanical Engineers, Paper 86-GT-132, 1986.
[34] Chyu, M. K., Hsing, Y. C., Shih, T. I. P., and Natarajan, V., "Heat Transfer Contributions of Pins and Endwall in Pin-Fin Arrays: Effects of Thermal Boundary Condition Modeling," *Journal of Turbomachinery*, Vol. 121, No. 2, 1999, pp. 257–263.
[35] Lau, S. C., Han, J. C., and Kim, Y. S., "Turbulent Heat Transfer and Friction in Pin Fin Channels with Lateral Flow Ejection," *Journal of Heat Transfer*, Vol. 111, No. 1, 1989, pp. 51–58.
[36] Goldstein, R. J., Cho, H. H., and Jabbari, M. Y., "Effect of Plenum Crossflow on Heat (Mass) Transfer Near and Within the Entrance of Film Cooling Holes," *Journal of Turbomachinery*, Vol. 119, No. 4, 1997, pp. 761–769.